Journal of Drug Delivery Science and Technology 53 (2019) 101125

Contents lists available at ScienceDirect

Journal of Drug Delivery Science and Technology

journal homepage: www.elsevier.com/locate/jddst

Novel fatty acid-based pH-responsive nanostructured lipid carriers for enhancing antibacterial delivery

Nawras Osman[a], Calvin A. Omolo[a], Ramesh Gannimani[a], Ayman Y. Waddad[a], Sanjeev Rambharose[a], Chunderika Mocktar[a], Sanil Singh[b], Raveen Parboosing[c], Thirumala Govender[a,*]

[a] Discipline of Pharmaceutical Sciences, School of Health Sciences, University of KwaZulu-Natal, Private Bag X 54001, Durban, 4000, South Africa
[b] Biomedical Resource Unit, University of KwaZulu-Natal, Private Bag X 54001, Durban, 4000, South Africa
[c] Department of Virology, University of KwaZulu-Natal/National Health Laboratory Service (NHLS), Private Bag X03, Mayville, 4058, KwaZulu-Natal, South Africa

ARTICLE INFO

Keywords:
pH-responsive
Nanostructured lipid carriers
Vancomycin
Methicillin-resistant
Staphylococcus aureus (MRSA)

ABSTRACT

The present study is aimed at the employment of novel fatty acid derived lipids for the preparation of pH-responsive nanostructured lipid carriers (NLCs) for vancomycin (VCM) intravenous delivery against resistant and sensitive *Staphylococcus aureus* bacteria. Two branched lipids [stearic acid derived solid lipid and oleic acid derived liquid lipid] were synthesized, characterized and used to fabricate NLCs by hot homogenization technique. Particle size, polydispersity index, zeta potential and encapsulation efficiency were 225.2 ± 9.1 nm, 0.258 ± 0.02, −9.2 ± 2.7 mV and 88.7 ± 13.12%, respectively. An understanding of drug encapsulation efficiencies and formation of the NLCs were supported by *in silico* studies. *In vitro* antibacterial activity revealed that VCM loaded-NLCs had higher activity against methicillin-susceptible and resistant *Staphylococcus aureus* than the bare VCM. Cell viability study showed that NLCs had 2.5-fold better killing percentage than the bare drug at similar concentrations. Furthermore, the *in vivo* efficacy of VCM loaded-NLCs was assessed in a mouse model of MRSA skin infection. MRSA CFU load of the skin treated with NLCs was 37-fold lower than bare VCM ($p < 0.05$). This novel pH-responsive NLCs may, therefore, show potential for efficient and enhanced antibiotic delivery.

1. Introduction

The golden era of antibiotic discovery was followed by the emergence of drug resistance, which has become a considerable health threat globally and has led to higher medical costs for individuals, community and the government [1,2]. Infectious organisms have developed resistance to multiple classes of antibiotics [3], most concerning are nosocomial and community-associated methicillin-resistant *Staphylococcus aureus* (MRSA) infections, which pose a growing therapeutic challenge, and are associated with raised risks of treatment failure and mortality rates [4]. Although vancomycin (VCM) has been the most effective antibiotic against MRSA [5], there are several reports of resistance and therapy failure, highlighting the need for new strategies to enhance its activity and prevent the spread of resistance [6].

Nano drug delivery systems (NDDS) have shown potential to improve conventional dosage forms, having increased drug concentration at the infection site [7], sustained and targeted release of antibiotics [6], thereby improving intended therapeutic outcomes [8]. These systems have been shown to enhance the efficacy of antibiotics, reduce their side effects and overcome resistance to antibiotics [9], thus providing a viable approach to overcome dosage form related issues attributed to the development of antibiotic resistance [10].

One of the novel drug delivery systems that has attracted much attention recently is the nanostructured lipid carriers (NLCs). Since their introduction, around 30 products are commercially available in the market [11,12]. They attract more attention in drug delivery due to their ability to incorporate both hydrophilic and hydrophobic drugs, enable simple large-scale production and improve drug loading capacity [13]. However, there are limited reports towards the application of NLCs for delivery of antibiotics, therefore, there is a need to explore this system for antibiotics delivery. Encapsulating of antibiotics via NLCs with lipids having inherent antibacterial activity will offer the advantages of NLCs as a drug delivery system at the same time improve the efficacy of the loaded antibiotic [14].

Due to the versatility in their formulation NLCs have been formulated to respond to different stimuli such as pH, temperature [15]

* Corresponding author.
E-mail address: govenderth@ukzn.ac.za (T. Govender).

https://doi.org/10.1016/j.jddst.2019.101125
Received 25 February 2019; Received in revised form 9 May 2019; Accepted 18 June 2019
Available online 20 June 2019
1773-2247/

and light with programmed drug release [16]. pH-responsive nanosystems are one of the most promising drug delivery systems as changes in pH are associated with disease conditions, such as cancer [17], inflammation [18], and bacterial infections [19]. Numerous studies have been reported for pH-responsive systems for NLCs, however, most reported studies have been in tumor targeting [20] and ocular drug delivery [15].

Literature survey has also show reports on pH-responsive antibiotic drugs delivery systems [21]. Our group has previously reported pH-responsive lipidic nano drug delivery systems such as liposomes, composed of fatty acids with three hydrocarbon tails and a secondary amine group [22] and SLNs systems using acid cleavable and linear lipids [23,24]. Developing NLCs with surface charge switching (anionic to cationic) properties in acidic media can enhance cationic fusion with the anionic bacterial cell wall, thereby facilitating the availability of higher antibiotic concentration at the bacterial site [25]. Thus, pH-responsive-NLCs with branched lipids for delivery systems can enhance antibiotic delivery with high encapsulation efficiency and sustained release [26] and could go a long way in formulating antibiotics delivery systems which can help to combat the rampant antimicrobial resistance.

We herein report a pH-responsive NLCs formulated from two novel fatty acid based branched lipids for intravenous delivery of vancomycin drug. We believe that this is the first study that reports the delivery of an antibiotic employing these synthesized materials and via a pH-responsive NLCs. The aim of this study was therefore to employ an ion-pairing strategy to formulate pH-responsive novel VCM loaded NLCs incorporating branched solid and liquid lipids. Stearic acid derived solid lipid (SASL), composed of two stearyl tails and bis β-alanine heads and oleic acid derived liquid lipid (OALL) with two tails of oleic acid and a primary amine head were proposed.

We envisage that pH responsiveness can be introduced into NLCs via a combination of fatty acid derived solid lipid containing a carboxylic acid group, and a liquid lipid containing a primary amino group which can form an ion pair by electrostatic interaction. These interactions are mainly influenced by the pH-dependent ionization property of both acid and base in aqueous solution. In addition, the branching of the bi fatty acyl tails of lipids proposed in this study could add to the stability of NLCs, as branched fatty acids have been shown to form a strong lipid matrix for higher encapsulation efficiency and controlled release [27]. Furthermore, the fatty acid derived lipids have been shown to increase bacterial membrane permeability and inherent antimicrobial activity against a wide range of bacteria, including MRSA [28], hence their use could be an added advantage for this study. *In vitro*, *in vivo,* and *in silico* studies are reported in this study.

2. Materials and methods

2.1. Materials

Stearic acid and Serinol were procured from Sigma-Aldrich (UK), while Trifluoroacetic Acid (TFA), di-tert-butyl dicarbonate (t-Boc) and N, N′-dicyclohexyl carbodiimide (DCC) were obtained from Merck (Germany). Tertiary butyl acrylate (TBA) and triisopropylsilane (TIPS) were purchased from Sigma-Aldrich (Germany). Nutrient Broth and Mueller Hinton Agar (MHA) were bought from Biolab Inc. (South Africa), Vancomycin hydrochloride, oleic acid (OA), 4-(Dimethylamino) pyridine (DMAP), Mueller Hinton broth 2 (MHB), dialysis tubing cellulose membrane and all other materials were procured from Sigma-Aldrich (USA). Vancomycin hydrochloride was converted to the vancomycin free base (VCM), according to a previously reported method [14]. Milli-Q purified water was obtained from an Elix® water purification system Millipore Corp. (USA). Bacterial strains used were *Staphylococcus aureus* (Rosenbach) (ATCC®BAA-1683) (MRSA) and *Staphylococcus aureus* (ATCC 25922) (SA).

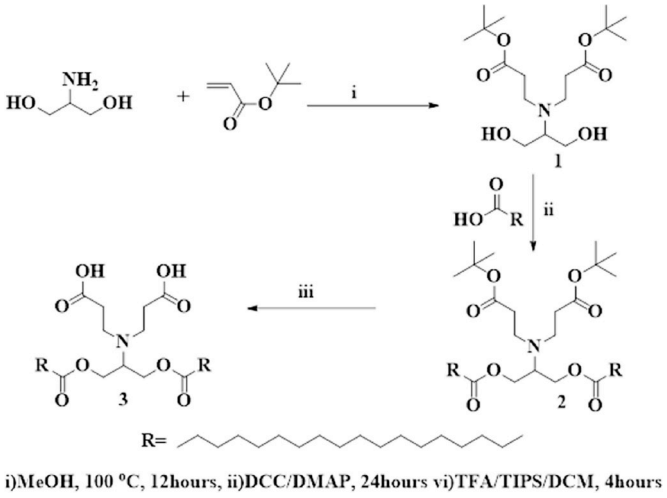

Scheme 1. Synthesis of stearic acid derived solid lipid (SASL).

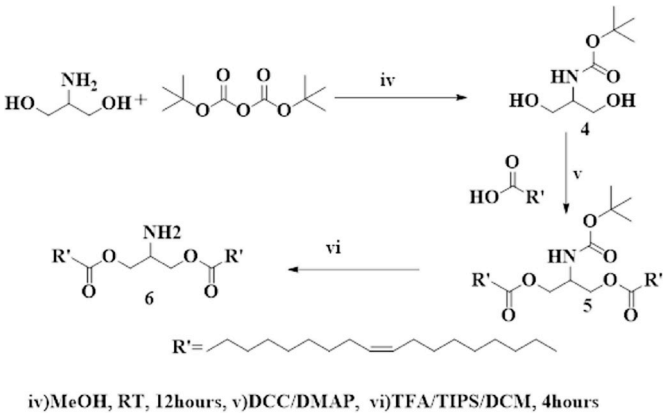

Scheme 2. Synthesis of oleic acid derived liquid lipid (OALL).

2.2. Synthesis and characterization of the branched lipids

The lipids were synthesized as per the following scheme, Scheme 1, Scheme 2.

Synthetic procedure and structural elucidation can be found in the supplementary material (Supplementary material).

2.3. In vitro cytotoxicity

The cytotoxic effects of SASL and OALL were assessed on three cell lines namely Human embryonic kidney (HEK-293), liver (HEP G2) and lung epithelial (A549) following a previously reported method [29]. The cell lines were cultured in growth medium supplemented with penicillin/streptomycin (1 %) solution and fetal bovine serum (10%). The cells were incubated in a humidified incubator with an atmosphere of 5% CO_2 for 24 h at 37 °C. Thereafter, SASL and OALL samples were dissolved in dimethyl sulfoxide and diluted with distilled water to make 20, 40, 60, 80 and 100 µg/ml concentration. Following the exponential growth phase, the cell lines were collected and seeded equivalently (2.4×10^3) into a 96 well culture plate, followed by incubation for 24 h to allow cell adherence. Thereafter, the spent media was removed and fresh medium containing test samples (100 ml per well) was added. Following incubation, the culture medium was removed and replaced with fresh culture medium and MTT solution (100 µl each). After 4 of incubation, the culture medium and MTT reagents were aspirated and the formazan crystals were solubilized by adding 100 µl dimethyl sulfoxide per well before measuring the absorbance at 540 nm using a microplate spectrophotometer (Spectrostar nano, Germany). Culture

medium with cells only and without cells used as the negative control and blank respectively. All experiments were replicated six times and the percentage of viable cells was calculated using equation (1):

$$\%\ Cell\ viability = \left(\frac{A\ 540\ nm\ treated\ cells}{A\ 540\ nm\ untreated\ cells}\right) \times\ 100 \quad (1)$$

2.4. Preparation of VCM-SAOA-NLCs

As previously reported hot homogenization followed by ultrasonication method was employed to prepare the VCM loaded SASL and OALL pH-responsive NLCs (VCM-SAOA-NLCs) [30]. Briefly, the lipid phase, consisting of a total of 500 mg of SASL and OALL lipids in varying ratios (0.5:1, 1:1 and 2:1) and VCM (20 mg), were mixed and melted at a temperature above the lipid melting point. 250 mg of Tween 80 was dissolved in distilled water (20 ml) and heated separately to the same temperature. Both phases were then mixed and homogenized using Ultra Turrax T-25 homogenizer (IKA Labortechnik, Germany) for 15 min at 6000 rpm. The resultant emulsion was sonicated at 30% amplitude for 10 min and subsequently cooled using an ice-water bath. Subsequently, the distilled water was added to adjust the final volume up to 20 ml. Blank (drug-free)-SAOA-NLCs was prepared using the same technique, with batches being prepared in triplicate.

2.5. Size, polydispersity index (PDI), zeta potential (ZP) and morphology

Dynamic light scattering technique using a Zeta-sizer Nano ZS90 instrument (Malvern Instruments Ltd., UK) at 25 °C was used to measure the size, PDI and ZP of VCM-SAOA-NLCs. NLCs samples were appropriately diluted and measured in triplicate. For morphological studies, VCM-SAOA-NLCs was diluted and a solution of 1% uranyl acetate (UA) was used for negative staining. The stained samples were deposited on a copper grid and air-dried before visualization using a transmission electron microscope TEM (JOEL JEM-1010, Japan) operated at 100 kV accelerating voltage [31].

2.6. Entrapment efficiency (EE) and drug loading (DL)

In order to determine the EE and DL of VCM-SAOA-NLCs, the ultrafiltration technique was used [14]. Briefly, Amicon® Ultra-4 centrifugal filter tubes (Millipore Corp., USA) of 10 kDa pore size was filled with NLCs suspension (3 ml) followed by centrifugation for 45 min at 2000 rpm at 25 °C. A validated High-Pressure Liquid Chromatography (HPLC) (Shimadzu, Japan) method was used [7] to quantify the unentrapped VCM in the filtrate, UV detection was carried out at 280 nm. A mixture of [0.1% trifluoroacetic acid in water and acetonitrile (85/15 v/v)] with a flow rate of 1 ml/min and 100 µl injection volume was pumped through Nucleosil 100-5 C18 column (150 mm x 4.6 mm internal diameter). The HPLC method showed linearity of the calibration curve in the range between 10 and 100 µg/ml, the regression coefficient (R^2) was 0.9915. The following equations were used to obtain the EE (%) and DL (%).

$$EE\ (\%) = \left(\frac{The\ weight\ of\ VCM\ in\ NLCs}{The\ weight\ of\ VCM\ added}\right) \times\ 100 \quad (2)$$

$$DL\ (\%) = \left(\frac{The\ weight\ of\ VCM\ in\ NLCs}{Total\ weight\ of\ nanoparticles}\right) \times\ 100 \quad (3)$$

2.7. Thermal profiles

VCM, SASL, freeze-dried drug loaded NLCs and physical mixture thermal profiles were investigated using a differential scanning calorimeter (DSC-60, Shimadzu, Japan). Briefly, appropriate quantities of the samples were placed in a sealed aluminum pan, and scanning was performed at an increment rate of 10 °C/min over a temperature range of 30 °C–300 °C under a nitrogen atmosphere, with a flow rate of 10 ml/min. An empty aluminum pan was used as a reference [32].

2.8. In vitro drug release and release kinetics

The *in vitro* release profile of VCM loaded pH-responsive NLCs was investigated using the dialysis bag method [33]. In order to achieve sink condition, a dialysis tube (pore size:14000 Da) containing 2 ml of VCM-SAOA-NLCs was placed in 40 ml PBS solutions of pH 6 and 7.4 at 37 °C in an incubator with 100 rpm shaking speed. 3 ml of the samples were withdrawn at predetermined time intervals and replaced with equivalent quantities of fresh PBS solution (pH 6 and 7.4) to maintain a constant volume. According to the method mentioned in section 2.6, the amount of VCM released at each time interval was determined using HPLC. Drug release kinetics of VCM-SAOA-NLCs were investigated using various mathematical models, including zero order, first order, Higuchi, Hixson-Crowell, Weibull, and Korsmeyer–Peppas. The best fit model was obtained by calculating the root means square error (RMSE) and correlation coefficient (R^2), while the release mechanism was determined by calculating the value of the release exponent (n) in Korsmeyer–Peppas model. The parameters of the *in vitro* drug release kinetics were investigated using the DDSolver software program.

2.9. In silico interaction of VCM and lipids carriers

An *in-silico* study was undertaken to understand the interactions between VCM and lipid carriers (SASL and OALL), as well as the effect of lipid ratio on the EE of VCM in the presence of a constant ratio of Tween 80 as a stabilizer [34]. Biovia Materials Studio (MS) 2016 installed on the remote server at the Centre for High-Performance Computing (CHPC) (Cape Town South Africa) was used to perform all molecular modeling techniques. VCM structure (PDB:1SHO) was obtained from the protein data bank website, while SASL and OALL were constructed using PerkinElmer ChemDraw (version 15), and the Tween 80 structure was obtained from PubChem website (CID 443315), after which hydrogen atoms were added to all structures and then their geometry was cleaned.

All structures were optimized to their lowest energy conformations using the smart minimizer algorithm available in the forcite module of MS software. A COMPASS force field was typed, and the convergence tolerance criteria were set to 0.001 kcal/mol during the geometrical optimization study, whilst the molecular dynamics (MD) study was performed in a vacuum. All VCM, SASL, OALL and Tween 80 structures were initially placed inside the cubic cell (10 × 10 × 10 nm). After geometry optimization, the system periodic boundary was stabilized and the MD simulation of over 50 ps was performed at room temperature. In order to understand the effect of the lipid ratio on EE, all the MD studies were conducted in two different ratios namely 2:1 and 1:1 for SASL and OALL, respectively. The final assembled structures were then studied to understand the intermolecular interactions and various forces that contributed to complex formation.

2.10. In vitro antibacterial activity

Broth dilution method was used to determine the minimum inhibitory concentration (MIC) of bare VCM, VCM-SAOA-NLCs and the blank (drug-free)-SAOA-NLCs against SA and MRSA at pH 7.4 and 6 [35]. Bacterial cultures were grown at 37 °C for 18 h in Nutrient Broth in a shaking incubator (Labcon, USA) at 100 rpm. A concentration equivalent to 0.5 McFarland's Standard using a DEN-1B McFarland densitometer (Latvia) was achieved by diluting the bacterial cultures with sterile distilled water. This was further diluted to 1:150 with sterile distilled water to achieve a final concentration of 5×10^5 colony forming units (CFU)/ml. Serial dilutions of bare VCM and VCM-SAOA-NLCs were prepared in MHB (pH 7.4 and 6), inoculated with

diluted bacterial cultures and incubated at 37 °C in a shaking incubator at 100 rpm for 18 h. After incubation, 10 µl of the test samples were spotted onto MHA and incubated at 37 °C for 18 h, this process was repeated daily for five days, all tests were performed in triplicate. The blank-SAOA-NLCs (negative control) and bare VCM (positive control) were subject to the same as VCM-SAOA-NLCs.

2.11. Bacterial cell viability assay

Flow cytometry technique was performed to quantify viable MRSA cells [36]. Bacteria were treated with VCM solution (positive control) at MIC of 7.8 and 0.98 µg/ml and VCM-SAOA-NLCs at the MIC of 0.98 µg/ml, followed by incubation at 37 °C for 6 h. Untreated MRSA cells were utilized as a negative control [37]. 50 µl of VCM solution and VCM-SAOA-NLCs broth were added to flow cytometry tubes contained sheath liquid (350 µl) followed by vortexing for 5 min [38]. The mixture was then stained with 5 µl of Propidium iodide (PI) (membrane impermeant) and Syto9 (membrane permeant) for 30 min. BD FACSCANTO II flow cytometer (Becton Dickinson, USA) was used in this study, with minimally 10,000 cells being gathered.

2.12. In vivo antibacterial activity and histological evaluation

In vivo antibacterial activity assessment employed the use of a mouse skin infection model was used to further evaluate anti-MRSA activity of the optimal VCM-SAOA-NLCs formulation, as per the protocol described previously [35]. Male BALB/c mice (18–20 g) were obtained from the Biomedical Research Unit at the University of KwaZulu-Natal. A day before the experiment, the back skins of the mice were shaved and disinfected with 70% ethanol. On the day after, the mice were divided into three groups of four mice each: negative control, positive control, and treatment group. Thereafter 50 µl of MRSA was diluted in saline solution to achieve a concentration of 1.5×10^8 CFU/ml and administered intradermally. The positive control and treatment groups were injected 30 min later at the same infected site with bare VCM and VCM-SAOA-NLCs respectively, while the negative control group was injected with the MRSA only. The mice were observed for 48 h under the normal condition of 12 h light-darkness cycle at 19–23 °C temperature with adequate ventilation and relative humidity of 55 ± 10%. Thereafter, the mice were sacrificed, and the infected skin was harvested and homogenized in 5 ml of PBS (pH 7.4). PBS was used to serially dilute the tissue homogenates, after which 20 µl were spotted onto on nutrient agar plates and incubated at 37 °C for 24 h and the CFU was determined.

Histological evaluations were conducted on the excised skin from the injection site, with the skin samples being transferred directly after harvesting and excision from normal saline into 10% buffered formalin. After seven days, the skin samples were subjected to dehydration in an ethanol gradient and embedded in paraffin wax. Microtome (Leica RM2235, Leica Biosystems, Germany) was then used to obtain tissue sections from tissue wax blocks, with the sections being collected on slides, dried and stained with hematoxylin and eosin (H&E). The sections were examined and captured with a Leica Microscope DM 500 that was fitted with a Leica ICC50 HD camera (Leica Biosystems, Germany). All the animal experiments were performed in accordance with the protocol approved by the Animal Research Ethics Committee of the University of KwaZulu-Natal (Approval number. AREC/104/015PD).

2.13. Statistical analysis

One-way analysis of variance (ANOVA) followed by Bonferroni's multiple comparison tests using GraphPad Prism® 6 (GraphPad Software Inc., USA) were used for statistical analysis. The variance was considered significant when the p-value was < 0.05, with the results being expressed as a mean ± standard deviation (SD).

3. Results and discussion

3.1. Synthesis and characterization of the lipids

The solid lipid SASL was synthesized in three steps. The first step involved the bis-aza-Michael addition of tertiary butyl acrylate to serinol to form compound 1, which was confirmed by both ^{1}H NMR and ^{13}C NMR. The appearance of a strong multiplet at δ 1.37 ppm integrating for 18 protons in ^{1}H NMR, and the appearance of carbon peaks at δ 28, 35, 80 and 172 in ^{13}C NMR, representing isobutane carbons, -CH2C═O-, C$(CH_3)_3$-COO - and C═O, confirmed the formation of compound 1. The second step involved the coupling of the two free hydroxyl groups on compound 1 with stearic acid using DCC/DMAP chemistry to obtain compound 2. The product was confirmed by the appearance of aliphatic peaks at δ 0.808 (multiplet), δ 1.18 (multiplet) and δ 1.53 (multiplet) on ^{1}H NMR. The third step involved hydrolyzation of the tertiary butyl esters of compound 2 to form SASL, using TFA and TIIPS as scavengers to avoid any possible side reactions. The successful synthesis of SASL was confirmed by the disappearance of isobutane peaks at 1.4 ppm in ^{1}H NMR and at 28 ppm in ^{13}C NMR.

For the OALL synthesis, firstly, the amine group on serinol was protected using di-ter-butyl dicarbonate (t-Boc) and the product confirmed by both ^{1}H NMR and ^{13}C NMR. A peak appeared at δ 1.34 ppm in ^{1}H NMR, which integrated to 9 protons, while the peak at δ 28.3 ppm in ^{13}C NMR confirmed the isobutane chain. In addition, a peak at δ 156. 4 ppm confirmed the presence of carbonyl group of boc amide which confirmed the t-Boc protection of an amino group of serinol (compound 4). Compound 4 was coupled with oleic acid using DCC and DMAP as catalysts to yield compound 5. In ^{1}H NMR, the characteristic peaks at δ 0.803–0.837 ppm and peaks at δ 5.28 to 5.299 represented terminal -CH_3, and olefinic protons of oleic acid respectively, confirming the synthesis of compound 5 as these peaks integrated to their expected theoretical calculated protons (supplementary material). Compound 5 was subjected to Boc deprotection using TFA and TIIPS to obtain compound 6 as OALL. The disappearance of isobutane peaks at δ 1.4 ppm in ^{1}H NMR and at δ 28 ppm in ^{13}C NMR indicated the successful cleavage of boc deprotection and confirmed the successful synthesis of OALL.

3.2. In vitro cytotoxicity

A cytotoxicity study was performed to determine the biosafety of the newly synthesized lipids. MTT results showed that the synthesized novel lipids SASL and OALL displayed a high percentage (> 75%) cell viability after 48 h exposure across the concentration range studied (Fig. 1). SASL and OALL displayed cell viability between 77.55 and 94.83% and 75.70 to 87.20%, respectively (Fig. 1A and B respectively). Although the % cell viability decreased slightly at the higher concentrations, no clear dose-dependent trends were observed for either SASL or OALL across all the tested cell lines (Fig. 1). According to the relative growth rate (RGR), the toxicity grade of both the SASL and OALL was found to be grade 1, in which the cell viabilities greater than 75% are regarded as noncytotoxic [39]. Thus, SASL and OALL are considered as safe for biomedical application.

3.3. Preparation of drug loaded NLCs

Once structure and biosafety of SASL and OALL were confirmed, their potential for VCM loaded NLCs formation was then explored. VCM-SAOA-NLCs were prepared from the OALL (liquid lipid) and SASL (solid lipid), Tween 80 as a surfactant, and VCM by hot homogenization followed by ultrasonication. Preliminary studies were performed using different ratios of lipids and surfactant to obtain a formulation with optimal size, PDI and acceptable switch from negative to the positive charge in different pH with maximum entrapment efficiency of the VCM (Table 1).

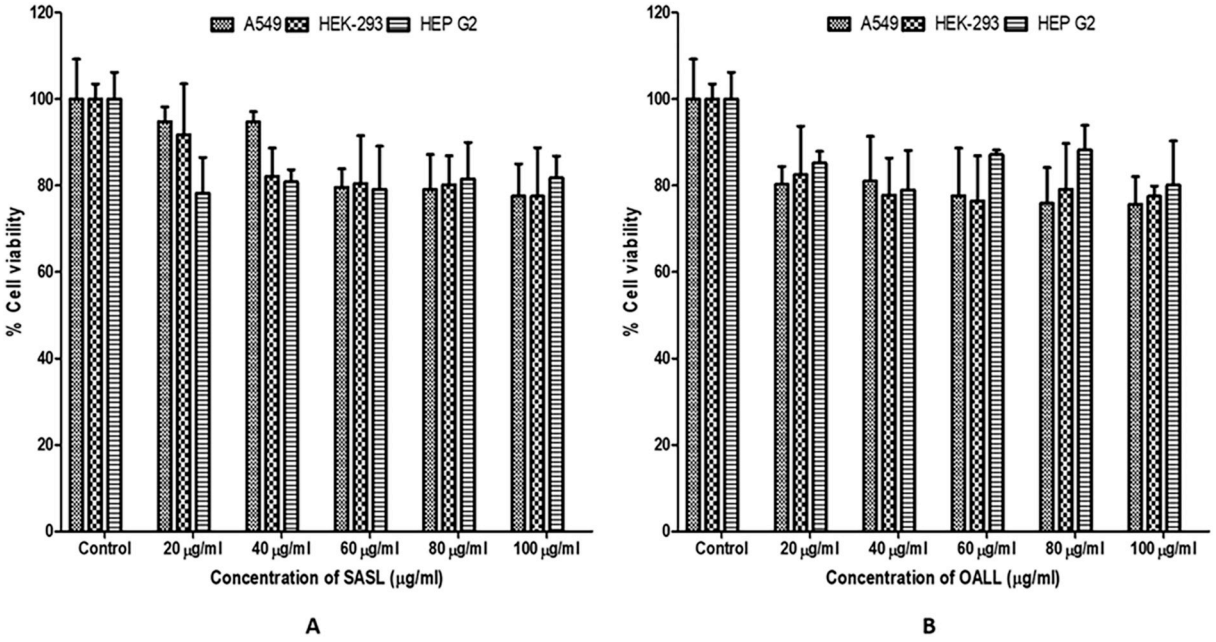

Fig. 1. Cytotoxicity evaluation of various concentrations of A) SASL B) OALL against A 549, HEK-293, and HEP G2 cells. .

Table 1
Particle size, PDI, and ZP of VCM-SAOA-NLCs.

SASL: OALL ratio	pH	Particle size (nm)	PDI	ZP (mV)	EE %
0.5:1	7.4	555.7 ± 76.3	0.70 ± 0.27	−4.7 ± 0.7	
	6.0	798.6 ± 318	0.72 ± 0.28	−2.8 ± 0.9	57.23 ± 3.0
	4.5	854,7 ± 125	0.75 ± 0.20	11.0 ± 1.3	
1:1	7.4	290.3 ± 20	0.36 ± 0.08	−7. 4 ± 1.3	
	6.0	358.3 ± 38	0.49 ± 0.06	0.2 ± 0.3	69.25 ± 2
	4.5	442.8 ± 80	0.49 ± 0.40	12.1 ± 0.4	
2:1	7.4	225.2 ± 9.1	0.258 ± 0.02	−9.2 ± 2.7	
	6.0	322.4 ± 37.7	0.386 ± 0.02	3.37 ± 0.8	88.7 ± 13.12
	4.5	458.7 ± 6	0.431 ± 0.04	9.8 ± 0.4	

At pH 7.4, as the solid lipid: liquid lipid ratio increased from 0.5:1 to 2:1, the particle size and PDI of the NLCs decreased from 555.7 nm to 225.2 nm and 0.7 to 0.2, respectively, whereas the ZP values changed from −4.7 mV to −9.2 mV, while the EE percentage improved from 57% to 88%. The increase in particle size, in accordance with an increase in liquid lipid content, may have led to an increase in the viscosity and consequently the NLCs swelling [40].

Alternatively, the higher solid lipid to liquid lipid ratios formed more stable nanoparticles with homogeneous size distributions and enhanced EE. The size, PDI, ZP, and EE of VCM-SAOA-NLCs formulations were similar to other reported NLCs using fatty acids lipids [41,42] and confirmed the ability of the newly synthesized lipids to form VCM loaded NLCs.

The VCM-SAOA-NLCs formulation with a solid lipid: liquid lipid ratio of 2:1 displayed a size, PDI, and ZP of 225.2 ± 9.1 nm, 0.258 ± 0.02, −9.2 ± 2.7 mV respectively. The EE (%) and DL (%) for this VCM-SAOA-NLCs were found to be 88.7 ± 13.12% and 3.55 ± 0.52% respectively. This entrapment was higher than other reported pH-responsive lipid-based drug delivery systems from our group [22–24,43].

This enhanced EE (%) could be due to the high partitioning of the hydrophobic VCM free base in the lipid matrix. In addition, the SASL has two carboxylic arms, which increase the ion-pairing between the solid lipid and VCM, leading to high entrapment and the branching of the lipid could have provided a better matrix for encapsulation [26]. Similar results were reported, where ion-pairing mechanism enhanced the EE (%) of poorly soluble drugs in solid lipid nanoparticles [44] and polymeric nanoparticles [45]. Thus, the VCM-SAOA-NLCs system consisting of a solid lipid: liquid lipid ratio of 2:1 was considered the optimal formulation, as it had the lowest size, smallest PDI and highest stability with highest EE (%) and was therefore characterized further.

3.4. Characterization of the optimal VCM-SAOA-NLCs

To obtain more information about the size and morphology of the VCM-SAOA-NLCs TEM study was performed and demonstrated that VCM-SAOA-NLCs had a well-defined spherical shape with an average size of 235.6 nm, which correlated well with the results of the dynamic light scattering technique (Fig. 2). These results were comparable to other NLCs reported [46].

To determine the pH responsiveness, VCM-SAOA-NLCs were dispersed in buffer solutions with different pH ranges (7.4, 6 and 4.5). The

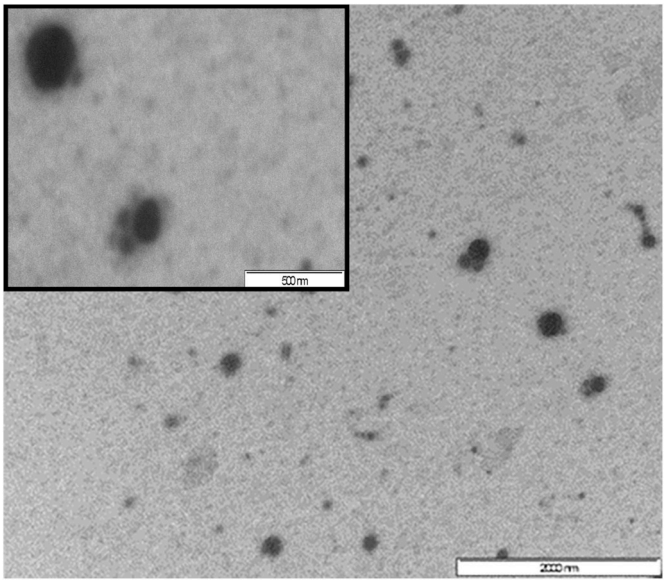

Fig. 2. Morphology of VCM-SAOA-NLCs.

optimal formulation showed pH responsiveness in terms of size, PDI, and ZP (Table 1). At pH 7.4, 6 and 4.5, the VCM-SAOA-NLCs size increased from 225.2 nm to 322.4 nm and 458.7 nm respectively, the PDI increased from 0.258 to 0.386 and 0.431 respectively, and the ZP also switched from −9.2 ± 2.7 mV to +3.37 mV and +9.8 mV, respectively.

In the VCM-SAOA-NLCs, the primary amine group of OALL binds to the carboxylic acid group of SALL by proton exchange ionic interaction [47]. At pH 7.4, the NLCs are negatively charged due to the carboxylate ions of the SASL on the NLCs surface. At low pH, due to the high concentration of H^+ ions, both the amine group of OALL and the carboxylate group of SASL remain protonated, which results in a breakage of the ionic interaction between the two lipids [48]. This phenomenon was demonstrated by the positive ZP at low pH. The breakage of the ion pair bridge between the two lipids minimizes their affinity to each other, causing the disassembly of the NLCs-dispersion and an eventual increase in their hydrodynamic diameter. The above change in size signifies a change in the conformational structure of the NLCs, while the switch from negative to positive charge is expected to have an influence on increasing the drug release and promoting interactions with the negatively charged bacterial cell wall for enhancing antibacterial activity [25,49].

3.5. VCM-SAOA-NLCs thermal analysis

The DSC study was undertaken to investigate the crystallinity and the thermal behavior of the NLCs components. The thermal profiles of SASL, VCM, lyophilized VCM-SAOA-NLCs and the physical mixture of VCM and SASL were compared (Fig. 3). The endothermic peaks of SASL and VCM were observed at 71.53 °C and 103.40 °C respectively, and the physical mixture showed almost similar thermal behavior to the individual components. While the peak for the lyophilized VCM-SASL-NLCs appeared at 62.57 °C and the VCM peak disappeared, which could be attributed to its transformation from the crystalline form into the amorphous form, as it was entrapped within the NLCs matrix [50].

3.6. In vitro release of optimal VCM-SAOA-NLCs

The *in vitro* release profile of the VCM solution and VCM-SAOA-NLCs were investigated using the dialysis bag diffusion technique at pH 7.4 and pH 6. At pH 7.4 the VCM solution release was almost complete within the first 24 h, while the VCM-SAOA-NLCs released only 47% at the same time point (Fig. 4). In comparison with the VCM solution, the

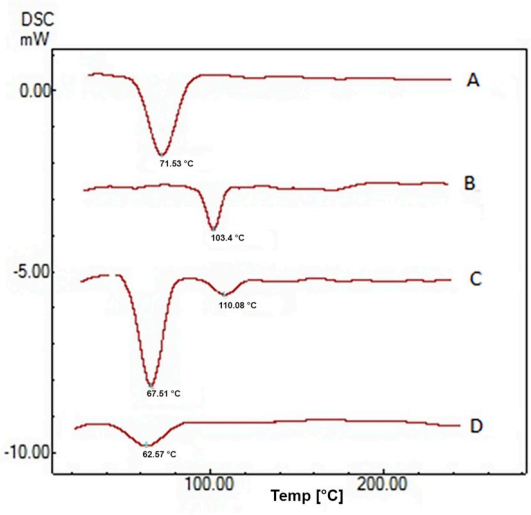

Fig. 3. DSC thermogram of (A) SASL (B) VCM (C) physical mixture of VCM and SASL and (D) lyophilized VCM-SAOA-NLCs. .

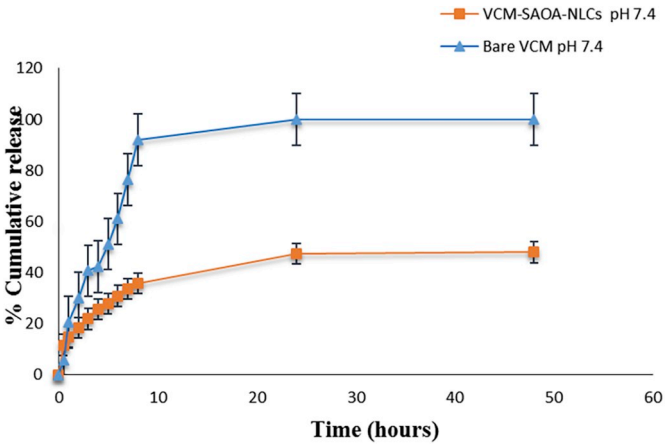

Fig. 4. *In vitro* drug release profiles of bare VCM and VCM-SAOA-NLCs at pH 7.4 \ (n = 3). .

VCM-SAOA-NLCs release was slower, indicating sustained release profiles. These results were better than our previously reported lipidic systems where it took only 8 h to release 74.89% at acidic pH [24].

VCM-SAOA-NLCs prolonged-release could be attributed to the lipid matrix of the VCM-SAOA-NLCs, which retain the hydrophobic VCM free base for a longer time [14]. In addition, the fatty acids long carbon chain length and matric formed from the branching might have slowed the diffusion rate of the drug, resulting in slower drug release [51], which could be beneficial for prolonged and sustained antibacterial activity [52].

While the VCM-SAOA-NLCs release was similar up to the 4th h at both pH conditions (Fig. 5), it had a statistically significant ($p < 0.05$) faster release at pH 6 than at pH 7.4 up to 48 h. This higher release at lower pH was attributed to the protonation of OALL and SASL in acidic media, leading to a breakage of the ion pair between the two lipids, and the nanoparticles hydrodynamic diameter increasing due to electrostatic repulsion between the lipids. This resulted in the NLCs swelling and breaking, leading to higher and faster drug release. Similar results were obtained by our group, whereby VCM release from the pH-responsive solid lipid nanoparticles was higher and faster at acidic media compared to the physiologic pH [23]. This pH-sensitive release behavior is significant for enhanced VCM protection at physiologic pH, improved drug release, enhanced localization, and bioavailability at the acidic infection sites, thus improving the antibacterial activity [25].

For kinetic analysis, the release data of the optimized VCM-SAOA-NLCs was fitted into zero order, first order, Higuchi, Hixson-Crowell, Korsmeyer–Peppas and Weibull models (Table 2). Although the VCM-

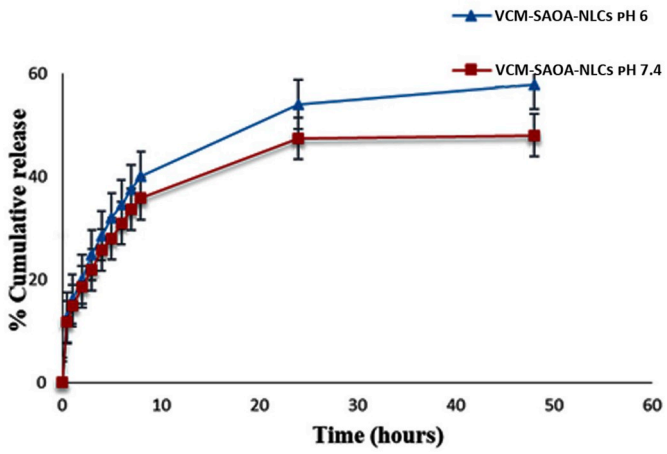

Fig. 5. Effect of pH on drug release profiles of VCM-SAOA-NLCs (n = 3).

Table 2
Release kinetics data from different models.

Model	Equation	R^2		RMSE		Release exponent (n)	pH 7.4	pH 6	pH 7.4
		pH 6	pH 7.4	pH 6					
Zero Order	$Q = k.\ t + Q_0$	1.460	−1.783	22.218	20.075				
First Order	$Q = Q_0 .\ e^{kt}$	−0.018	−0.600	14.185	15.219				
Higuchi	$Q = k.\ t^{½}$	0.625	0.495	8.667	8.542				
Korsmeyer-Peppas	$Q = k.\ t^{n}$	0.936	0.913	3.601	3.531		0.308	0.289	
Hixson-Crowell	$Q^{⅓} = kt + Q_0^{⅓}$	−0.377	−1.003	16.517	17.025				
Weibull	$Q = 1\ \exp\ [-(t)a/b]$	0.961	0.935	2.801	3.043				

R^2 = linear regression coefficient, RMSE = Root mean square error.

SAOA-NLCs release was higher at pH 6, it had similar kinetic behavior to the release at pH 7.4. The highest R^2 values were 0.94 and 0.961, while the lowest root means square error (RMSE) values were 3.04 and 2.89 at pH 7.4 and pH 6, respectively. Thus, the Weibull model was considered the best fit model for the VCM-SAOA-NLCs release at both pH conditions.

The Weibull exponent parameter (β) value is used to interpret the drug release mechanism, with $\beta \leq 0.75$ indicating a Fickian diffusion, and $0.75 < \beta < 1$ indicating a combined mechanism, whereas a β value higher than 1 is associated with the complex release mechanism. The values of the exponent parameter (β) for VCM-SAOA-NLCs were 0.37 and 0.418 at pH 7.4 and pH 6 respectively, indicating Fickian diffusion as the release mechanism. These results were consistent with the (n) values of Korsmeyer-Peppas model, whereas (n) values at pH 7.4 and pH 6 and were 0.289 and 0.308, respectively, confirming the Fickian mechanism of VCM release from the VCM-SAOA-NLCs, as the (n) value was less than 0.5 [53,54].

3.7. In silico interaction of VCM and lipids carriers

Molecular modeling was used to investigate the interaction of VCM with the SAOA-NLCs system and the effect of the solid to liquid lipid ratio on VCM entrapment efficiency. The potential energy of VCM free base, SASL, OALL and Tween 80 were found to be 1509.249, 590.150, 354.144 and 213.780 kcal/mol respectively. Stable molecules, with final energies of 123.318, −164.488, −47.506, and −1.317 kcal/mol for VCM, SASL, OALL and Tween 80, respectively were obtained by geometry optimization using the smart minimizer algorithm in the forcite module. The molecular dynamics (MD) study for the 2:1 lipid ratio indicated the possible formation of VCM-SAOA-NLCs. Mass of the complex potential energy increased from 866.075 kcal/mol to 1367.44 kcal/mol at the end of the MD simulation (Fig. 6 A). This energy increase as a phase transformation of the individual components of the NLCs occurred indicated the formation of a stable VCM-SAOA-NLCs complex [55].

When the ratio of the solid lipid to liquid lipid was 1:1, the potential energy was found to be 1603.991 kcal/mol by the end of the MD study, and the VCM was observed to interact with Tween 80 rather than the SASL or OALL (Fig. 6 B). However, in case of a 2:1 ratio the potential energy was 1367.44 kcal/mol and the VCM was incorporated into the SASL (Fig. 6 A) rather than repelled out, as in the case of 1:1 ratio. The low potential energy of the complex is essential for its stability. The significance of the low potential energy of a 2:1 ratio is indicated by the incorporation of VCM into the SASL leading to more stable complex compared to a 1:1 ratio complex where VCM was expelled out of the NLCs. This observation may explain the higher EE (%) of VCM at solid lipid: liquid lipid of 2:1 compared to the lower EE (%) when the solid lipid: liquid lipid ratio was 1:1 (Table 1) and can be explained by the competition between the liquid lipid and the VCM to interact with the solid lipid. Increasing the solid lipid quantity might have led to higher partitioning of the VCM free base in the lipid, as the SASL has two carboxylic arms, which increases the ion pairing between the solid lipid and VCM, subsequently improving the EE [14]. These studies showed the possibility of formation of a stable NLCs system and identified the possible mechanism behind the higher EE (%) with a higher ratio of the solid lipid (SASL) than the liquid lipid (OALL).

3.8. In vitro antibacterial activity

The *in vitro* antibacterial activities of bare VCM, VCM-SAOA-NLCs

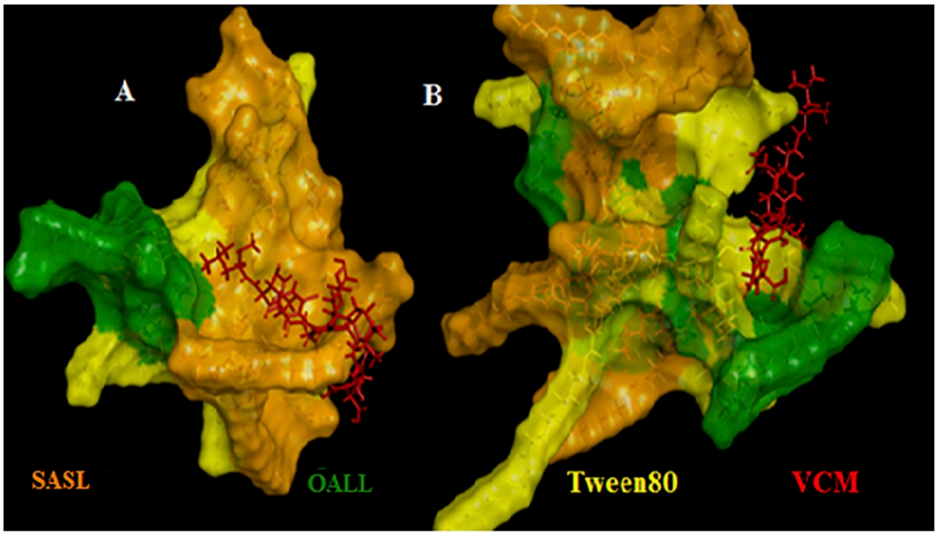

Fig. 6. The multivalent binding phenomenon of SASL, OALL and Tween 80 with VCM. (A) Solid lipid: liquid lipid is 2:1 (B) Solid lipid: liquid lipid is 1:1.

Table 3
In vitro antibacterial activity of the formulations at pH 7.4 and pH 6.

In vitro antibacterial activity at pH 7.4								
Time (h)	24	48	72	96	24	48	72	96
	SA (MIC μg/ml)				MRSA (MIC μg/ml)			
Bare VCM	3.9	250	NA	NA	7.8	NA	NA	NA
VCM-SAOA-NLCs	1.95	1.95	1.95	3.9	1.95	1.95	1.95	1.95
Blank- SAOA-NLCs	NA	NA	NA	NA	NA	NA	NA	NA
In vitro antibacterial activity at pH 6								
Time (h)	24	48	72	96	24	48	72	96
	SA (MIC μg/ml)				MRSA (MIC μg/ml)			
Bare VCM	3.9	500	NA	NA	7.8	NA	NA	NA
VCM-SAOA-NLCs	0.488	0.488	1.95	3.9	0.98	0.98	1.95	7.8
Blank-SAOA-NLCs	NA	NA	NA	NA	NA	NA	NA	NA

NA = No activity. The values are expressed as mean ± SD (n = 3).

and the blank-SAOA-NLCs were investigated against SA and MRSA at pH 6 and 7.4 using a broth dilution method (Table 3). Bare VCM showed a MIC value of 3.9 μg/ml against SA at both pH conditions and increased to 7.8 μg/ml against MRSA at both pH conditions. The MIC values of VCM-SAOA-NLCs against SA were 1.95 μg/ml and 0.488 μg/ml, whereas the MIC values of VCM-SAOA-NLCs against MRSA were 1.95 μg/ml and 0.98 μg/ml at pH 7.4 and pH 6, respectively. These results showed that the VCM-SAOA-NLCs had lower MIC values, and thus superior antibacterial efficacy compared to the bare VCM against both SA and MRSA bacteria at both pH conditions. These results were superior to our previously reported study, whereby the pH-responsive SLNs had only 2-fold enhancement of activity against MRSA at acidic media compared to 8-fold enhancement reported in this study [23]. Furthermore, the VCM-SAOA-NLCs formulation activity was extended up to 96 h, while the bare VCM had an activity for only 48 h.

The enhanced extended anti-microbial activity, in comparison to the bare VCM, could be due to the small size with the large surface area, as well as the lipophilic nature of VCM-SAOA-NLCs, which could enable better penetration and uptake into the bacterial cell wall, thus enhancing the VCM activity [56]. In addition, the VCM-SAOA-NLCs release over a prolonged period of time (Fig. 5) could have contributed to the extended activity of up to 96 h compared to the bare VCM [57]. Additionally, the lipids contained the oleic acid moiety, which could have been attributed to the enhanced activity of VCM-SAOA-NLCs [58]. It has also been reported that fatty acids tend to accumulate in the membrane of bacteria thus interfering with the normal membrane functions and growth [59]. Thus, having a system with the highly branched lipidic system might have a similar effect and enhance the activity of VCM.

Importantly, the VCM-SAOA-NLCs had lower MIC values at pH 6 compared to pH 7.4 against both SA and MRSA bacteria. At pH 6, the VCM-SAOA-NLCs activity was four and two times better against SA and MRSA respectively than at pH 7.4. The superior antibacterial activity of the VCM-SAOA-NLCs at acidic pH compared to pH 7.4 may be due to the protonation of the VCM-SAOA-NLCs and ion pair bridge breakage, and hence have a higher VCM release at the acidic site. In addition, the VCM-SAOA-NLCs surface charge switching to positive in acidic media can enhance the binding of the VCM-SAOA-NLCs with the anionic bacterial cell wall, and therefore release higher VCM concentrations at the acidic infection site, subsequently increasing its uptake by the bacteria cell wall and reducing the total number recovered. This strategy will, therefore, play a key part in minimizing the emergence of bacterial resistance [25].

3.9. Bacterial cell viability assay

The MRSA viable cells were determined using an earlier reported method with slight modifications [37]. Two gates were drawn, one representing live cells in the population and the other, beyond the fluorescence of viable cells, representing cells that internalized PI (dead cells). The effect of VCM and VCM-SAOA-NLCs at their respective MICs (7.8 μg/ml and 0.98 μg/ml respectively) on the MRSA cells was investigated by plotting a PI fluorescence log versus a Syto 9 log (Fig. 7). [36]. The results showed that after incubation, the MRSA with the bare VCM and VCM-SAOA-NLCs at their respective MICs had 65.2 ± 2.33 %

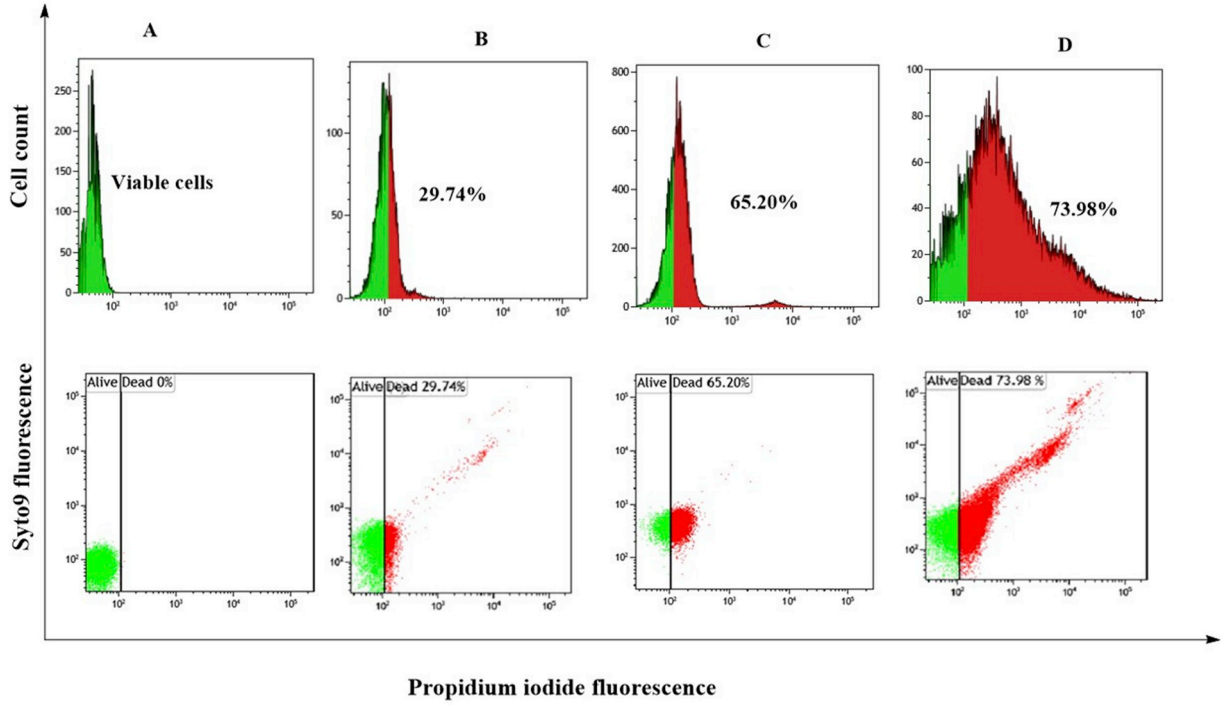

Fig. 7. Dot plots of flow cytometry data of subpopulation phenotypes of MRSA cells after treatment E) MRSA cells (negative control), F) MRSA cells treated with bare VCM at 0.98 μg/ml, G) MRSA cells treated with bare VCM at its MIC (7.8 μg/ml) and H) MRSA treated VCM-SAOA-NLCs at its respective MIC (0.98 μg/ml). .

and 73.98 ± 1.72% death was observed. Interestingly, for the MRSA cells treated with bare VCM at a concentration similar to MIC of VCM-SAOA-NLCs (0.98 μg/ml), there were only 29.74 ± 1.03% dead cells (Fig. 7) compared to 73.98% of the NLCs formulation. This finding is noteworthy, as VCM-SAOA-NLCs had a better killing effect, although the concentration was 8-fold lower compared to the bare VCM MIC. Therefore, these results indicate that VCM-SAOA-NLCs could be employed as a treatment option to bare VCM that offers better therapeutic outcomes, with fewer dose-dependent side effects associated with VCM.

3.10. *In vivo* antibacterial activity

Having confirmed the *in vitro* antibacterial activity of the VCM-SAOA-NLCs formulation, *in vivo* studies were performed. The BALB/c mouse skin infection models were used to further evaluate the VCM-SAOA-NLCs activity against MRSA, its counts being 151600, 30000 and 800 CFU/ml for untreated, bare the VCM and VCM-SAOA-NLCs groups respectively. These results further reflect the enhanced activity of the VCM-SAOA-NLCs against MRSA compared to the bare VCM.

There was a statistically significant ($p < 0.05$) reduction in the MRSA counts that remained in the skin of the mice treated with VCM-SAOA-NLCs and bare VCM compared to the untreated group. The bacterial burdens were 189- and 5-fold less in the mice skin treated with VCM-SAOA-NLCs and bare VCM respectively than the untreated group. Furthermore, there was a 37-fold decrease ($P < 0.05$) in the bacterial populations treated with VCM-SAOA-NLCs compared to that of bare VCM (Fig. 8).

These results confirmed VCM-SAOA-NLCs superior anti-MRSA activity to the bare VCM, which can be related to the small nanoparticle size, large surface area and hydrophobicity of the NLCs that enhance the MRSA bacterial membrane binding capacity and permeability. Moreover, oleic acid is able to enhance penetration across the bacteria cell wall in addition to its inherent anti-MRSA activity [58], thereby possibly contributing to enhanced activity.

The NLCs as a nanocarrier enhance its delivery in a sustained manner, thus ensuring higher concentrations at the site of action [60]. At acidic infection sites, the VCM-SAOA-NLCs protonation might have led to the surface charge switching to positive, which can improve binding to the negatively charged MRSA cell wall and enhance VCM uptake. Subsequently, increasing the VCM binding to the terminal D-Ala-D-Ala residues targeted site, resulting in the bacterial cell wall synthesis inhibition and the MRSA colonization reduction [25]. Thus, pH-responsive VCM-SAOA-NLCs can be an effective multifunctional delivery system that can be used to enhance the efficacy of VCM and

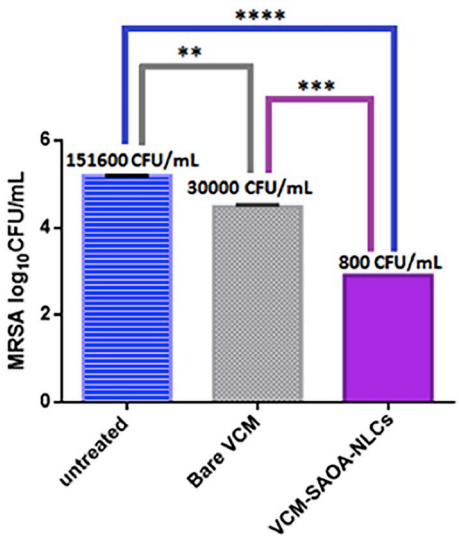

Fig. 8. *In vivo* anti-MRSA activity. Data are presented as mean ± SD (n = 3).

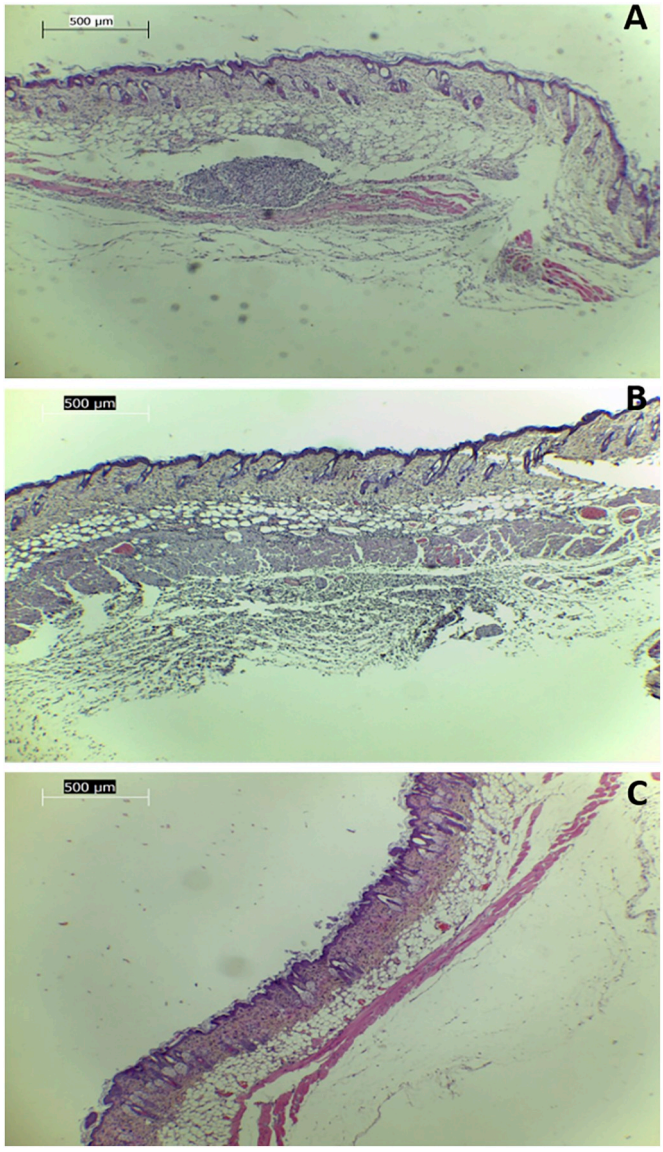

Fig. 9. Light microscopy images of H&E stained samples of (A) untreated (B) bare.

other antibiotics against resistant bacteria, with the added advantage of reducing the high dose-dependent toxicity of antibiotics, thereby improving treatment outcomes and patient compliance.

To further evaluate the skin integrity and morphological changes, histological analysis was performed on all skin samples. Light microscopy analysis of the Hematoxylin and Eosin (H&E (stained slides showed evidence of inflammation and abscess formation at the infection sites of the untreated and bare VCM groups (Fig. 9 A and B respectively). The skin samples of these groups presented with swelling of the dermal layer and the presence of white blood cells at the inflammation site. However, there were no signs of abscess formation, and only minimal evidence of tissue inflammation in the skin samples of the VCM-SAOA-NLCs treated group (Fig. 9C).

In the untreated group, a large portion of the tissue at the infection site was infiltrated by the bacteria, as evidenced by the degree of the inflammatory response at the infection site (Fig. 9 A). This inflammatory response was also seen in the bare VCM treated samples but to a lesser extent. These findings correlated directly with the MRSA counts from the infection sites. The untreated group displayed the largest number of recovered bacteria and displayed the greatest degree of inflammation and abscess formation. The VCM-SAOA-NLCs treated

group displayed the least signs of inflammation and no abscess formation, which correlated with its statistically significant lower bacterial load. However, the bare VCM group presented a statistically significantly larger number of isolated bacteria than the VCM-SAOA-NLCs treated group and displayed more histomorphological signs, indicating tissue inflammation and abscess formation. These histological assessments additionally confirm the superior antibacterial activity of the VCM-SAOA-NLCs compared to the bare VCM.

4. Conclusion

In this study, pH-responsive branched lipids were successfully synthesized and novel NLCS were formulated for enhanced VCM drug delivery to the acidic infectious site. VCM-SAOA-NLCs with a small size, low PDI and high EE from novel lipids were successfully prepared and showed pH responsiveness in terms of size and surface charge switching at acidic pH. Drug release was higher at pH 6, which was attributed to the protonation of both the OALL and SASL components of NLCs, leading to a breakage of the ion pair between them, and the subsequent swelling of NLCs. *In silico* studies supported the higher EE of VCM at a solid lipid: liquid lipid ratio of 2:1 (1603.991 kcal/mol) than 1:1 (1367.44 kcal/mol) this may be due to the higher affinity of the VCM with the solid lipid than the liquid lipid. The *in vitro* antibacterial activity against SA and MRSA revealed that the NLCs activity was enhanced at pH 6 compared to pH 7.4 and bare drug. Furthermore, *in vivo* BALB/c mouse skin infection models revealed that there was a 37-fold reduction in the MRSA colony forming unit load in the mice skin treated with VCM-SAOA-NLCs compared to that treated with bare VCM. Histological investigations further confirmed the antimicrobial efficiency of the VCM-SAOA-NLC, as it showed minimal signs of tissue inflammation and abscess formation. Therefore, from the present work, it could be concluded that as lipids, OALL and SASL showed the potential for preparing pH-responsive VCM loaded NLCs with enhanced activity against SA and MRSA.

Conflicts of interest

The authors declare that there is no conflict of interest.

Acknowledgment

The authors acknowledge the University of KwaZulu-Natal (UKZN), UKZN Nanotechnology Platform and the National Research Foundation of South Africa for financial support. We also thank Biomedical Resource Unit (BRU), Microscopy and Microanalysis Unit (MMU), Flow Cytometry Research Laboratory and Department of Human Physiology at UKZN for technical assistance and Ms. Carrin Martin and Charlotte Ramadhin for proofreading.

Appendix A. Supplementary data

Supplementary data to this article can be found online at https://doi.org/10.1016/j.jddst.2019.101125.

References

[1] S.J. Leopold, F. van Leth, H. Tarekegn, C. Schultsz, Antimicrobial drug resistance among clinically relevant bacterial isolates in sub-Saharan Africa: a systematic review, J. Antimicrob. Chemother. 69 (2014) 2337–2353.
[2] S. Lehtinen, F. Blanquart, N.J. Croucher, P. Turner, M. Lipsitch, C. Fraser, Evolution of antibiotic resistance is linked to any genetic mechanism affecting bacterial duration of carriage, Proc. Natl. Acad. Sci. U. S. A. 114 (2017) 1075–1080.
[3] A.P. Magiorakos, A. Srinivasan, R.B. Carey, Y. Carmeli, M.E. Falagas, C.G. Giske, S. Harbarth, J.F. Hindler, G. Kahlmeter, B. Olsson-Liljequist, D.L. Paterson, L.B. Rice, J. Stelling, M.J. Struelens, A. Vatopoulos, J.T. Weber, D.L. Monnet, Multidrug-resistant, extensively drug-resistant and pandrug-resistant bacteria: an international expert proposal for interim standard definitions for acquired resistance, Clin. Microbiol. Infect. 18 (2012) 268–281.
[4] N.V. Ayala-Núñez, H.H.L. Villegas, L.d.C.I. Turrent, C.R. Padilla, Silver nanoparticles toxicity and bactericidal effect against methicillin-resistant Staphylococcus aureus: nanoscale does matter, NanoBiotechnology 5 (2009) 2–9.
[5] S.P. Chakraborty, S.K. Sahu, S.K. Mahapatra, S. Santra, M. Bal, S. Roy, P. Pramanik, Nanoconjugated vancomycin: new opportunities for the development of anti-VRSA agents, Nanotechnology 21 (2010) 105103.
[6] A.J. Huh, Y.J. Kwon, "Nanoantibiotics": a new paradigm for treating infectious diseases using nanomaterials in the antibiotics resistant era, J. Control. Release 156 (2011) 128–145.
[7] Y.-Y. Jiang, G.-T. Tang, L.-H. Zhang, S.-Y. Kong, S.-J. Zhu, Y.-Y. Pei, PEGylated PAMAM dendrimers as a potential drug delivery carrier: in vitro and in vivo comparative evaluation of covalently conjugated drug and noncovalent drug inclusion complex, J. Drug Target 18 (2010) 389–403.
[8] C.L.J.P. Ventola, Therapeutics, Progress in nanomedicine: approved and investigational nanodrugs, PT 42 (2017), pp. 742–755.
[9] J.M. Caster, A.N. Patel, T. Zhang, A. Wang, Nanobiotechnology, Investigational nanomedicines in 2016: a review of nanotherapeutics currently undergoing clinical trials, Wiley Interdiscip. Rev. Nanomed. Nanobiotechnol. 9 (2017) e1416.
[10] B.D. Brooks, A.E. Brooks, Therapeutic strategies to combat antibiotic resistance, Adv. Drug Deliv. Rev. 78 (2014) 14–27.
[11] M.A. Iqbal, S. Md, J.K. Sahni, S. Baboota, S. Dang, J. Ali, Nanostructured lipid carriers system: recent advances in drug delivery, J. Drug Target. 20 (2012) 813–830.
[12] D. Pandita, A. Munjal, S. Godara, V. Lather, Nanocarriers in drug and gene delivery, Advances in Animal Biotechnology and its Applications, Springer, 2018, pp. 71–102.
[13] C.-Y. Zhuang, N. Li, M. Wang, X.-N. Zhang, W.-S. Pan, J.-J. Peng, Y.-S. Pan, X. Tang, Preparation and characterization of vinpocetine loaded nanostructured lipid carriers (NLC) for improved oral bioavailability, Int. J. Pharm. 394 (2010) 179–185.
[14] R.S. Kalhapure, C. Mocktar, D.R. Sikwal, S.J. Sonawane, M.K. Kathiravan, A. Skelton, T. Govender, Ion pairing with linoleic acid simultaneously enhances encapsulation efficiency and antibacterial activity of vancomycin in solid lipid nanoparticles, Colloids Surfaces B Biointerfaces 117 (2014) 303–311.
[15] Y. Yu, R. Feng, S. Yu, J. Li, Y. Wang, Y. Song, X. Yang, W. Pan, S. Li, Nanostructured lipid carrier-based pH and temperature dual-responsive hydrogel composed of carboxymethyl chitosan and poloxamer for drug delivery, Int. J. Biol. Macromol. 114 (2018) 462–469.
[16] Y. Yang, X. Xie, Y. Yang, H. Zhang, X. Mei, Photo-responsive and NGR-mediated multifunctional nanostructured lipid carrier for tumor-specific therapy, J. Pharm. Sci. 104 (2015) 1328–1339.
[17] S. Li, Z. Su, M. Sun, Y. Xiao, F. Cao, A. Huang, H. Li, Q. Ping, C. Zhang, An arginine derivative contained nanostructure lipid carriers with pH-sensitive membranolytic capability for lysosomolytic anti-cancer drug delivery, Int. J. Pharm. 436 (2012) 248–257.
[18] H.-L. Pu, W.-L. Chiang, B. Maiti, Z.-X. Liao, Y.-C. Ho, M.S. Shim, E.-Y. Chuang, Y. Xia, H.-W.J.A.n. Sung, Nanoparticles with dual responses to oxidative stress and reduced pH for drug release and anti-inflammatory applications, ACS Nano 8 (2014) 1213–1221.
[19] R.S. Kalhapure, M. Jadhav, S. Rambharose, C. Mocktar, S. Singh, J. Renukuntla, T. Govender, pH-responsive chitosan nanoparticles from a novel twin-chain anionic amphiphile for controlled and targeted delivery of vancomycin, Colloids Surfaces B Biointerfaces 158 (2017) 650–657.
[20] C.H. Kim, C.-K. Sa, M.S. Goh, E.S. Lee, T.H. Kang, H.Y. Yoon, G. Battogtokh, Y.T. Ko, Y.W. Choi, ph-sensitive Pegylation of rIPl peptide-conjugated nanostructured lipid carriers: design and in vitro evaluation, Int. J. Nanomed. 13 (2018) 6661–6675.
[21] Y.Y. Yuan, C.Q. Mao, X.J. Du, J.Z. Du, F. Wang, J. Wang, Surface charge switchable nanoparticles based on zwitterionic polymer for enhanced drug delivery to tumor, Adv. Mater. 24 (2012) 5476–5480.
[22] M. Jadhav, R.S. Kalhapure, S. Rambharose, C. Mocktar, S. Singh, T. Kodama, T.J.C. Govender, p.o. lipids, Novel lipids with three C18-fatty acid chains and an amino acid head group for pH-responsive and sustained antibiotic delivery, Chem. Phys. Lipids 212 (2018) 12–25.
[23] R.S. Kalhapure, D.R. Sikwal, S. Rambharose, C. Mocktar, S. Singh, L. Bester, J.K. Oh, J. Renukuntla, T. Govender, Enhancing targeted antibiotic therapy via pH responsive solid lipid nanoparticles from an acid cleavable lipid, Nanomedicine 13 (2017) 2067–2077.
[24] D. Mhule, R.S. Kalhapure, M. Jadhav, C.A. Omolo, S. Rambharose, C. Mocktar, S. Singh, A.Y. Waddad, V.M. Ndesendo, T. Govender, Synthesis of an oleic acid based pH-responsive lipid and its application in nanodelivery of vancomycin, Int. J. Pharm. 550 (2018) 149–159.
[25] A.F. Radovic-Moreno, T.K. Lu, V.A. Puscasu, C.J. Yoon, R. Langer, O.C. Farokhzad, Surface charge-switching polymeric nanoparticles for bacterial cell wall-targeted delivery of antibiotics, ACS Nano 6 (2012) 4279–4287.
[26] M. Salim, H. Minamikawa, A. Sugimura, R.J.M. Hashim, Amphiphilic designer nano-carriers for controlled release: from drug delivery to diagnostics, Medchemcomm 5 (2014) 1602–1618.
[27] M.W. Meanwell, C. O'Sullivan, P. Howard, T.M. Fyles, Branched-chain and dendritic lipids for nanoparticles, Can. J. Chem. 95 (2016) 120–129.
[28] H.-H. Chen, W.-C. Huang, W.-H. Chiang, T.-I. Liu, M.-Y. Shen, Y.-H. Hsu, S.-C. Lin, H.-C. Chiu, pH-Responsive therapeutic solid lipid nanoparticles for reducing P-glycoprotein-mediated drug efflux of multidrug resistant cancer cells, Int. J. Nanomed. 10 (2015) 5035.
[29] S. Rambharose, R.S. Kalhapure, K.G. Akamanchi, T. Govender, Novel dendritic derivatives of unsaturated fatty acids as promising transdermal permeation enhancers for tenofovir, J. Mater. Chem. B 3 (2015) 6662–6675.
[30] A.R. Neves, M. Lucio, S. Martins, J.L. Lima, S. Reis, Novel resveratrol nanodelivery

systems based on lipid nanoparticles to enhance its oral bioavailability, Int. J. Nanomed. 8 (2013) 177–187.
[31] H. Shete, V. Patravale, Long chain lipid based tamoxifen NLC. Part I: preformulation studies, formulation development and physicochemical characterization, Int. J. Pharm. 454 (2013) 573–583.
[32] Y. Agrawal, K.C. Petkar, K.K. Sawant, Development, evaluation and clinical studies of Acitretin loaded nanostructured lipid carriers for topical treatment of psoriasis, Int. J. Pharm. 401 (2010) 93–102.
[33] A.Y. Waddad, S. Abbad, F. Yu, W.L. Munyendo, J. Wang, H. Lv, J. Zhou, Formulation, characterization and pharmacokinetics of Morin hydrate niosomes prepared from various non-ionic surfactants, Int. J. Pharm. 456 (2013) 446–458.
[34] S.J. Sonawane, R.S. Kalhapure, S. Rambharose, C. Mocktar, S.B. Vepuri, M. Soliman, T. Govender, Ultra-small lipid-dendrimer hybrid nanoparticles as a promising strategy for antibiotic delivery: in vitro and in silico studies, Int. J. Pharm. 504 (2016) 1–10.
[35] C.A. Omolo, R.S. Kalhapure, M. Jadhav, S. Rambharose, C. Mocktar, V.M. Ndesendo, T. Govender, Pegylated oleic acid: a promising amphiphilic polymer for nano-antibiotic delivery, Eur. J. Pharm. Biopharm. 112 (2017) 96–108.
[36] N.K. Shrestha, N.M. Scalera, D.A. Wilson, G.W. Procop, Rapid differentiation of methicillin-resistant and methicillin-susceptible Staphylococcus aureus by flow cytometry after brief antibiotic exposure, J. Clin. Microbiol. 49 (2011) 2116–2120.
[37] N.M. O'Brien-Simpson, N. Pantarat, T.J. Attard, K.A. Walsh, E.C. Reynolds, A Rapid and Quantitative flow cytometry method for the analysis of membrane disruptive antimicrobial activity, PLoS One 11 (2016) e0151694.
[38] M. Rüger, G. Bensch, R. Tüngler, U. Reichl, A flow cytometric method for viability assessment of Staphylococcus aureus and Burkholderia cepacia in mixed culture, Cytometry 81 (2012) 1055–1066.
[39] X. Cao, C. Cheng, Y. Ma, C. Zhao, Preparation of silver nanoparticles with antimicrobial activities and the researches of their biocompatibilities, J. Mater. Sci. Mater. Med. 21 (2010) 2861–2868.
[40] X. Lin, X. Li, L. Zheng, L. Yu, Q. Zhang, W. Liu, Preparation and characterization of monocaprate nanostructured lipid carriers, Colloids Surf A Physicochem Eng Asp 311 (2007) 106–111.
[41] F.-Q. Hu, S.-P. Jiang, Y.-Z. Du, H. Yuan, Y.-Q. Ye, S. Zeng, Preparation and characterization of stearic acid nanostructured lipid carriers by solvent diffusion method in an aqueous system, Colloids Surfaces B Biointerfaces 45 (2005) 167–173.
[42] H. Yuan, L.-L. Wang, Y.-Z. Du, J. You, F.-Q. Hu, S. Zeng, Preparation and characteristics of nanostructured lipid carriers for control-releasing progesterone by melt-emulsification, Colloids Surfaces B Biointerfaces 60 (2007) 174–179.
[43] S.S. Makhathini, R.S. Kalhapure, M. Jadhav, A.Y. Waddad, R. Gannimani, C.A. Omolo, S. Rambharose, C. Mocktar, T. Govender, Novel two-chain fatty acid-based lipids for development of vancomycin pH-responsive liposomes against Staphylococcus aureus and methicillin-resistant Staphylococcus aureus (MRSA), J. Drug Target. (2019) 1–14.
[44] G. Carneiro, E.L. Silva, L.A. Pacheco, E.M. de Souza-Fagundes, N.C.R. Corrêa, A.M. de Goes, M.C. de Oliveira, L.A.M. Ferreira, Formation of ion pairing as an alternative to improve encapsulation and anticancer activity of all-trans retinoic acid loaded in solid lipid nanoparticles, Int. J. Nanomed. 7 (2012) 6011.
[45] T.S.J. Kashi, S. Eskandarion, M. Esfandyari-Manesh, S.M.A. Marashi, N. Samadi, S.M. Fatemi, F. Atyabi, S. Eshraghi, R. Dinarvand, Improved drug loading and antibacterial activity of minocycline-loaded PLGA nanoparticles prepared by solid/oil/water ion pairing method, Int. J. Nanomed. 7 (2012) 221–234.
[46] Z. Shao, J. Shao, B. Tan, S. Guan, Z. Liu, Z. Zhao, F. He, J. Zhao, Targeted lung cancer therapy: preparation and optimization of transferrin-decorated nanostructured lipid carriers as novel nanomedicine for co-delivery of anticancer drugs and DNA, Int. J. Nanomed. 10 (2015) 1223.
[47] N.M. Pinkerton, A. Grandeury, A. Fisch, J.r. Brozio, B.U. Riebesehl, R.K. Prud'homme, Formation of stable nanocarriers by in situ ion pairing during block-copolymer-directed rapid precipitation, Mol. Pharm. 10 (2012) 319–328.
[48] F.F. Severin, I.I. Severina, Y.N. Antonenko, T.I. Rokitskaya, D.A. Cherepanov, E.N. Mokhova, M.Y. Vyssokikh, A.V. Pustovidko, O.V. Markova, L.S. Yaguzhinsky, Penetrating cation/fatty acid anion pair as a mitochondria-targeted protonophore, Proc. Natl. Acad. Sci. U. S. A. 107 (2010) 663–668.
[49] Y. Liu, H.J. Busscher, B. Zhao, Y. Li, Z. Zhang, H.C. van der Mei, Y. Ren, L. Shi, Surface-adaptive, antimicrobially loaded, micellar nanocarriers with enhanced penetration and killing efficiency in staphylococcal biofilms, ACS Nano 10 (2016) 4779–4789.
[50] D.R. Sikwal, R.S. Kalhapure, S. Rambharose, S. Vepuri, M. Soliman, C. Mocktar, T. Govender, Polyelectrolyte complex of vancomycin as a nanoantibiotic: preparation, in vitro and in silico studies, Mater Sci Eng C Mater Biol Appl 63 (2016) 489–498.
[51] S. Xie, L. Zhu, Z. Dong, X. Wang, Y. Wang, X. Li, W. Zhou, Preparation, characterization and pharmacokinetics of enrofloxacin-loaded solid lipid nanoparticles: influences of fatty acids, Colloids Surfaces B Biointerfaces 83 (2011) 382–387.
[52] A. Esmaeili, S. Ghobadianpour, Vancomycin loaded superparamagnetic MnFe2O4 nanoparticles coated with PEGylated chitosan to enhance antibacterial activity, Int. J. Pharm. 501 (2016) 326–330.
[53] J. Siepmann, N. Peppas, Modeling of drug release from delivery systems based on hydroxypropyl methylcellulose (HPMC), Adv. Drug Deliv. Rev. 64 (2012) 163–174.
[54] V. Papadopoulou, K. Kosmidis, M. Vlachou, P. Macheras, On the use of the Weibull function for the discernment of drug release mechanisms, Int. J. Pharm. 309 (2006) 44–50.
[55] A.T. Florence, D. Attwood, Physicochemical properties of drugs in solution, Physicochemical Principles of Pharmacy, Pharmaceutical press, London, UK, 2006, pp. 58–59.
[56] S. Ghaffari, J. Varshosaz, A. Saadat, F. Atyabi, Stability and antimicrobial effect of amikacin-loaded solid lipid nanoparticles, Int. J. Nanomed. 6 (2011) 35.
[57] X. Wang, S. Zhang, L. Zhu, S. Xie, Z. Dong, Y. Wang, W. Zhou, Enhancement of antibacterial activity of tilmicosin against Staphylococcus aureus by solid lipid nanoparticles in vitro and in vivo, Vet. J. 191 (2012) 115–120.
[58] C.-M. Huang, C.-H. Chen, D. Pornpattananangkul, L. Zhang, M. Chan, M.-F. Hsieh, L. Zhang, Eradication of drug resistant Staphylococcus aureus by liposomal oleic acids, Biomaterials 32 (2011) 214–221.
[59] C.H. Chen, Y. Wang, T. Nakatsuji, Y.-T. Liu, C. Zouboulis, R.L. Gallo, L. Zhang, M.-F. Hsieh, C.-M. Huang, An innate bactericidal oleic acid effective against skin infection of methicillin-resistant Staphylococcus aureus: a therapy concordant with evolutionary medicine, J. Microbiol. Biotechnol. 21 (2011) 391–399.
[60] B. Li, K.V. Brown, J.C. Wenke, S.A. Guelcher, Sustained release of vancomycin from polyurethane scaffolds inhibits infection of bone wounds in a rat femoral segmental defect model, J. Control. Release 145 (2010) 221–230.